Coherent bremsstrahlung from relativistic electrons in quasicrystals

R. Fusina
Code 7252, Naval Research Laboratory, Washington, DC 20375-5000

J. B. Langworthy
3114 Gracefield Road, No. 112, Silver Spring, Maryland 20904

A. W. Sáenz
Department of Physics, Catholic University of America, Washington, DC 20064
and Code 6390, Naval Research Laboratory, Washington, DC 20375-5000

(Received 24 October 2000; published 25 September 2001)

In this paper we develop a Born-approximation theory of coherent bremsstrahlung (CB) production by relativistic electrons in icosahedral quasicrystals (IQCs), described by a schematic model that incorporates the presence of phonon and phason disorder. Our main result is a formula for the cross section $d\sigma_{\mathrm{CB}}/dk$ of this process, differential with respect to the photon energy k. It predicts intense low-energy CB emission (type-*A* CB) when an electron is incident on an IQC along a direction almost, but not exactly, parallel to that of a major axis. It also entails a scaling law that could serve as a powerful experimental signature of type-*A* CB emitted by these IQCs and more general ones. We illustrate our theory by discussing numerical results for type-*A* CB emitted by electrons of 5-MeV kinetic energy incident in a direction close to a fivefold axis of icosahedral Al-Mn-Si (*i*-Al-Mn-Si) described by the above model. These calculations predict the presence of CB macropeaks in $d\sigma_{\mathrm{CB}}/dk$ vs k, to which many smaller peaks contribute, and which should be experimentally detectable. This is also expected to be the case for other directions of incidence. Reasons for believing that the schematic model yields qualitatively correct predictions for this cross section for relativistic electrons incident on real *i*-Al-Mn-Si are stated.

DOI: 10.1103/PhysRevE.64.046505 PACS number(s): 41.60.−m, 78.70.En, 61.44.Br

I. INTRODUCTION

The purpose of the present paper is to initiate the theoretical study of coherent bremsstrahlung (CB) emitted by energetic electrons traversing quasicrystals (QCs). Before summarizing its contents, it may be helpful to discuss briefly CB produced by fast electrons in crystals. This type of of γ radiation has been extensively studied experimentally and theoretically during the last 40 years [1]. It occurs when a crystal target is irradiated with relativistic electrons whose incident momenta are parallel or almost parallel to major crystal axes or planes. There are two kinds of CB in crystals, the most common of which arises from ''free-free'' radiative transitions and the other from ''free-bound'' transitions [2,3]. In contrast, a related type of coherent γ radiation, channeling radiation, arises from ''bound-bound'' transitions [2]. Here ''free'' refers to electronic states described by plane-wave solutions of Dirac's equation for a free electron, which are good approximations to the corresponding exact solutions when the magnitude of the incident electron momentum **p** is sufficiently large. On the other hand, the term ''bound'' refers to electronic states which are solutions of Dirac's equation describing free motion along the direction of a major crystal axis to which **p** is almost parallel, and transversely bound in the plane perpendicular to this direction. We can distinguish two types of free-free CB in crystals: type *A* and type *B*. Roughly speaking, type-*A* CB is intense radiation lying in the lower portion of the CB spectrum that can be emitted when the incident electron momentum **p** is almost, but not exactly, parallel to a set of major crystal planes. Type-*B* CB is less intense, higher-energy radiation that can be emitted when **p** is approximately, or even exactly aligned, along a major crystal axis [4].

It is well known that QCs, although they are aperiodic, possess long-range order and that their atoms are distributed along lines and planes analogous to those in crystals [5]. It is therefore natural to expect that fast electrons traversing QCs in appropriate directions can emit CB of types *A* and *B*, defined analogously to the corresponding types in crystals. It is thus very satisfying that type-*B* CB from a *T*-phase QC irradiated with 200- and 400-keV electrons has been detected at an electron microscope at the Max Planck Institute in Stuttgart [6]. In view of the great current interest in the study of properties of QCs, one expects that other experiments on accelerators and electron microscopes will be performed to investigate CB and CR production in these materials [7].

In this paper we will discuss a theory of CB emission from relativistic electrons traversing icosahedral quasicrystals (IQCs) with phonon and phason disorder [8] which are described by a simple model (*K* model). In particular, we will derive a Born-approximation formula for the cross section, differential with respect to photon energy, for CB production in such IQCs. Using this formula, we have calculated this cross section numerically for the case of type-*A* CB emitted by 5-MeV electrons incident on icosahedral Al-Mn-Si(*i*-Al-Mn-Si) (Ref. [9]). These calculations predict the presence of irregularly distributed macropeaks to which many smaller peaks contribute. Although the smaller peaks may not be individually observable, the macropeaks to which they give rise should be. These results are in strong contrast

with the regular distribution of peaks in the CB spectra from electrons traversing crystals. The corresponding cross sections for type-*A* or type-*B* CB in more realistic QC models are expected to exhibit similar properties. The feasibility of experimental detection of the above macropeaks is enhanced by the fact that our theory predicts that type-*A* CB obeys a distinctive scaling law that could serve as its experimental signature.

At present, about 100 intermetallic compounds of icosahedral quasicrystalline structure are known [10] as well as many such compounds with other types of quasicrystalline symmetries. However, complete structural information is lacking for many of them. A basic reason for this is that quasiperiodicity introduces too many structural variables for *x*-ray diffraction analyses to cope with [11]. All available methods will probably be needed in order to arrive at a satisfactory general understanding of the structure of QCs. This makes theoretical studies of CB production in QCs, such as the present one, especially timely, since they furnish an independent way of testing structural models experimentally.

This paper is organized as follows. In Sec. II we recall some basic quasicrystallographic facts which we use to define the *K* model. In addition, this section includes a discussion of the kinematics of CB from relativistic electrons traversing an IQC described by this model and a statement of the above cross-section formula for CB production in it. This formula is proved in Appendix B. In Sec. II we also define CB of types *A* and *B* from such IQCs and discuss their salient properties, including the scaling law for type-*A* CB alluded to earlier. The above-mentioned numerical results for *i*-Al-Mn-Si, as well as their analytical interpretation, are presented in Sec. III. In Sec. IV, the final section, we give reasons for expecting that these results differ only qualitatively from the corresponding ones for relativistic electrons incident on real *i*-Al-Mn-Si. We also mention an interesting topic for future research on CB emitted from QCs with no phason disorder. Appendixes A and C collect results needed in Sec. II, and in Appendix D we prove properties of CB peaks that are used in Sec. III. Finally, in Appendix E, we consider the effects of Landau-Pomeranchuk-Migdal and dielectric suppression [12,13] on our numerical predictions, concluding that most of the predicted CB peaks are unaffected by these phenomena. In future work, we intend to apply the present method to study coherent pair production in QCs.

II. THEORY OF CB FROM RELATIVISTIC ELECTRONS IN A MODEL IQC

A. Auxiliary quasicrystallographic facts and definition of the *K* model

The icosahedral quasilattice (IQL) considered can be generated by the cut-projection method [14,15], which we review briefly in this section both for the sake of completeness and to introduce useful notation. The experts will find nothing new here. The method will be applied to the six-dimensional simple cubic lattice

$$\Lambda=\left\{ a\sum_{i=1}^{6} m_i\boldsymbol{\varepsilon}_i ; m_i\in\mathbf{Z},\quad i=1,\ldots,6\right\} \tag{2.1}$$

of side length a, where $\{\varepsilon_i\}$ is the standard basis in $\mathbf{R}^6$ and $\mathbf{Z}$ denotes the integers. In this method, a projection operator Π (see Ref. [14], especially p. 184, where $\Pi=\pi$) maps $\mathbf{R}^6$ into a three-dimensional subspace $\mathcal{E}$ of $\mathbf{R}^6$ which is identified with ordinary physical space, while its orthogonal complement $\mathcal{E}'$ is commonly called perpendicular space. If $\mathbf{X}=\Pi\mathbf{Y}$ and $\mathbf{X}'=\Pi'\mathbf{Y}$, where $\mathbf{Y}\in\mathbf{R}^6$ and $\Pi'=I-\Pi$, we will say that $\mathbf{X}$, $\mathbf{X}'$ is a *complementary pair* or simply that these vectors are *complementary*. An important property of Π is that if $\mathbf{Y}\in\Lambda$, then the vectors of the complementary pair $\mathbf{X}$, $\mathbf{X}'$ are in 1-1 correspondence.

The model IQL of interest is defined as the set $\mathcal{K}$ of all points (vectors) $\mathbf{X}\in\mathcal{E}$ which belong to the set

$$L=\Pi\Lambda=\left\{ a\sum_{i=1}^{6} m_i\mathbf{e}_i : m_i\in\mathbf{Z},\quad i=1,\ldots,6\right\} \tag{2.2}$$

and whose unique complementary vectors $\mathbf{X}'\in\mathcal{E}'$ lie in an open triacontahedron $C(a)$ with center at the origin. Here $C(a)=\Pi'\gamma_6$, where γ_6 is the open six-dimensional cube $\gamma_6=\{(z_1,\ldots,z_6)\in\mathbf{R}^6: -a/2<z_i<a/2,\quad i=1,\ldots,6\}$ of side length a, centered at the origin [14,15]. The points of $\mathcal{K}$ are the vertices of prolate and oblate rhombohedrons which together tile $\mathcal{E}$ (Ammann tiles) [16]. A schematic model K_0 of a perfect static IQC is obtained by placing a single atomic species (Mn in our numerical calculations) at each of the vertices of the Ammann tiles of $\mathcal{K}$. This model has satisfactorily explained to first order the observed electron-diffraction patterns of icosahedral QCs [17,18] and has proved useful in studying the feasibility of ion channeling therein [19]. It can be viewed as a first step in constructing *K*, the more realistic disordered IQC, which we now define.

K belongs to an extensive class of disordered IQCs discussed by Jarić and Nelson [20]. Physically, it models an IQC in which phonons and phasons are thermalized, or in which the phasons have been quenched at a high temperature and the phonons thermalized at the lower quenching temperature. The reader will find further details in Ref. [20]. Formally, we identify *K* with a set of disordered realizations $K_{\mathbf{w}}$ of K_0 which are distributed in a Gaussian manner [20]. Each $K_{\mathbf{w}}$ is defined by the following two steps. First, for each pair $\mathbf{X}\in L$, $\mathbf{X}'\in L'=\Pi'\Lambda$ of complementary vectors, let $\mathbf{w}(\mathbf{X},\mathbf{X}')=\mathbf{u}(\mathbf{X})\oplus\mathbf{u}'(\mathbf{X}')$ be a random vector, where $\mathbf{u}(\mathbf{X})$ and $\mathbf{u}'(\mathbf{X}')$ are complementary. Then $\mathcal{K}_{\mathbf{w}}$ is defined as the discrete subset of L consisting of all vectors $\mathbf{X}+\mathbf{u}(\mathbf{X})(\mathbf{X}\in L)$ whose complementary vectors $\mathbf{X}'+\mathbf{u}'(\mathbf{X}')$ are in $C(a)$. Second, the disordered IQC $K_{\mathbf{w}}$ is obtained by placing an atom of a single atomic species at each site of $\mathcal{K}_{\mathbf{w}}$. In other words, $K_{\mathbf{w}}$ is the disordered version of K_0 obtained by displacing the atom at each tile vertex $\mathbf{X}$ of $\mathcal{K}$ by $\mathbf{u}(\mathbf{X})$. The random vectors $\mathbf{u}(\mathbf{X})$ and $\mathbf{u}'(\mathbf{X}')$ are interpreted as phonon and phason displacements, respectively.

B. CB kinematics and Born-approximation formula for $d\sigma_{\mathrm{CB}}/dk$

Before stating the formula for the cross section $d\sigma_{\mathrm{CB}}/dk$ of CB production by relativistic electrons incident of IQCs described by the K model, which is our main result, we consider some kinematical properties of the relevant CB.

The energy-momentum conservation laws for CB emitted by electrons traversing the disordered IQC K are expressed by the relations [21]

$$E=E'+k, \quad \mathbf{p}=\mathbf{p}'+\mathbf{k}+\mathbf{G} \quad (\mathbf{G}\in L^*). \tag{2.3}$$

Here $\mathbf{p},\mathbf{p}',\mathbf{k}$ denote the initial and final electron momenta and the photon momentum, respectively; $E=(p^2+m^2)^{1/2}$, $E'=(p'^2+m^2)^{1/2}$, $k=|\mathbf{k}|$ denote the corresponding energies, with $p=|\mathbf{p}|$, $p'=|\mathbf{p}'|$ and with m the electron rest mass; $\mathbf{G}$ denotes the momentum transfer to the quasilattice; and

$$L^*=\left\{(2\pi/a)\sum_{i=1}^{6} m_i\boldsymbol{\varepsilon}_i\in\mathbf{Z}, \quad i=1,\ldots,6\right\}. \tag{2.2$'$}$$

These laws are analogous to the corresponding ones for crystals [22]. They arise from the delta functions $\delta(\mathbf{q}-\mathbf{G})(\mathbf{G}\in L^*)$ occurring in $\langle|\tilde{\rho}_{\mathbf{w}}(q)|^2\rangle_0$ in Eq. (B9), where $\mathbf{q}=\mathbf{p}-\mathbf{p}'-\mathbf{k}$, and from $\delta(E-E'-k)$ in Eq. (B10).

In the relativistic regime ($\gamma\equiv E/m\gg 1$), the only vectors $\mathbf{G}$ in L^* contributing significantly to the CB from K are those with $|\mathbf{G}|\ll p$. Whence Eqs. (2.3) entail that for given $\mathbf{p}$ and $\mathbf{G}$ the energy of a CB photon emitted in the direction $\hat{\mathbf{k}}=\mathbf{k}/k$ is well approximated by

$$k=\frac{\mathbf{p}\cdot\mathbf{G}}{E-\mathbf{p}\cdot\hat{\mathbf{k}}+\hat{\mathbf{p}}\cdot\mathbf{G}}. \tag{2.4}$$

Using Eq. (2.4), one sees that for given $\mathbf{p}$ and $\mathbf{G}$ the energy of each emitted CB photon lies in the interval $0\leqslant k\leqslant k_{\mathbf{G}}(\hat{\mathbf{p}})$, where

$$k_{\mathbf{G}}(\hat{\mathbf{p}})=\frac{\mathbf{p}\cdot\mathbf{G}}{E-p+\hat{\mathbf{p}}\cdot\mathbf{G}}, \tag{2.5}$$

with $\hat{\mathbf{p}}=\mathbf{p}/p$. Hence $d\sigma_{\mathrm{CB}}/dk$, viewed as a function of k, drops sharply at each such $k_{\mathbf{G}}(\hat{\mathbf{p}})$, thus forming a peak. Equivalently, the only vectors $\mathbf{G}\in L^*$ contributing to the emission of CB photons of energy k for a given $\mathbf{p}$ are those for which

$$\hat{\mathbf{p}}\cdot\mathbf{G}\geqslant\Delta(x), \tag{2.6}$$

where $x=k/E$ and $\Delta(x)$ is the magnitude $p-p'-k$ of the minimum momentum transfer to K, which is accurately given by

$$\Delta(x)\cong\frac{(E-p)k}{p-k}\cong\frac{Ex}{2\gamma^2(1-x)} \tag{2.7}$$

in the relativistic regime. Since p will be fixed henceforth, the p dependence of $k_{\mathbf{G}}(\hat{\mathbf{p}})$ and $\Delta(x)$ has been omitted, as will also be done in the case of other p-dependent quantities.

Contrary to the case of the analogous CB cutoff energies for ordinary crystals, the $k_{\mathbf{G}}(\hat{\mathbf{p}})$ are dense in the kinematically allowed photon energy region $0<k\leqslant k_{\max}\cong E$. [This follows in a standard way from Eqs. (2.2) and (2.4), and the irrationality of $5^{1/2}$.] Most of the above drops in $d\sigma_{\mathrm{CB}}/dk$ are too small to be experimentally observable. However, for certain directions $\hat{\mathbf{p}}$ close to a QC direction (see Ref. [5]) it can happen that the $k_{\mathbf{G}}(\hat{\mathbf{p}})$ corresponding to an infinite number of distinct vectors $\mathbf{G}\in L^*$ coincide. This can lead to a large drop in $d\sigma_{\mathrm{CB}}/dk$, and hence to a large, observable peak [23]. We term such peaks *macropeaks*. (Concrete examples of macropeaks for type-A CB are given in Sec. III.) Large CB peaks in crystals have a similar origin; but while for directions $\hat{\mathbf{p}}$ close to appropriate crystal directions the distribution of these peaks falls into regular patterns, that of CB peaks in QCs is always irregular, due to the denseness of the $k_{\mathbf{G}}(\hat{\mathbf{p}})$.

The promised formula for the cross section $d\sigma_{\mathrm{CB}}/dk$ is

$$(k/N\sigma_0)(d\sigma_{\mathrm{CB}}/dk) = \sum_{\mathbf{G}\in L^*} F(\mathbf{G},x,\hat{\mathbf{p}})\exp(-2B|\mathbf{G}|^2 - 2B'|\mathbf{G}'|^2)|\tilde{\chi}(-\mathbf{G}')|^2, \tag{2.8}$$

and is derived in Appendix B [24]. Here N is the number of atoms in the IQC; $\sigma_0=z^2\alpha r_0^2$, where z is their atomic number, $\alpha\cong\frac{1}{137}$, and r_0 the classical electron radius; and $\exp(-2B|\mathbf{G}|^2)$, $\exp(-2B|\mathbf{G}'|^2)$ are the Debye-Waller factors arising from phonon and phason fluctuations, respectively [25]. We define $F(\mathbf{G},x,\hat{\mathbf{p}})$ as

$$F(\mathbf{G},x,\hat{\mathbf{p}})=\frac{|w(\mathbf{G})|^2\Delta(x)}{a^6V(a)}\frac{G_t^2}{G_l^2}\left\{1+(1-x)^2-\frac{4(1-x)\Delta(x)[G_l-\Delta(x)]}{G_l^2}\right\} \tag{2.9}$$

if $\mathbf{G}$ obeys condition (2.6) and as zero otherwise. In Eq. (2.9), $V(a)=2^{1/2}(1+\tau)(3-\tau)^{1/2}a^3$, the volume of the triacontahedron $C(a)$, where $\tau=(5^{1/2}+1)/2$; $G_l=\hat{\mathbf{p}}\cdot\mathbf{G}$, $G_t=(G^2-G_l^2)^{1/2}$, where $G=|\mathbf{G}|$; and $w(|\mathbf{G}|)=(1/\alpha z)\int_{\mathbf{R}^3}\exp(-i\mathbf{G}\cdot\mathbf{r})v(\mathbf{r})d\mathbf{r}$. Here $v(\mathbf{r})$ is the electron-atom interaction potential, which will be assumed to be of the Thomas-Fermi-Molière form [26]. Therefore,

$$w(\mathbf{G})=4\pi\sum_{i=1}^{3}\frac{\alpha_i}{(\beta_i/a_0)^2+G^2}, \tag{2.10}$$

where $(\alpha_1,\alpha_2,\alpha_3)=(0.10,0.55,0.35)$, $(\beta_1,\beta_2,\beta_3)=(6,1.2,0.3)$, and a_0 is the screening length in the Thomas-Fermi theory. Finally, $\tilde{\chi}$ denotes the Fourier transform of the characteristic function χ of $C(a)$ [27]. An exact formula for $\tilde{\chi}$ due to Elser [15] is stated as Eq. (C1) in Appendix C for the reader's convenience.

Naturally, B and B' will be assumed to be positive unless otherwise stated. Under this hypothesis, one can easily prove that the series (2.8) converges for all $\hat{\mathbf{p}}$ if $\mathbf{G}\in L^*$ and $0\leqslant x<x_{\max}$.

C. Definitions of CB of types *A* and *B*, and scaling law for type-*A* CB

In this section, we will consider a fixed, but arbitrary unit vector $\hat{\mathbf{d}}$ parallel to an IQC direction (axis) (Ref. [5]), Eq. (2.8) can be written in the form

$$(k/N\sigma_0)(d\sigma_{\mathrm{CB}}/dk)=S_A(x,\hat{\mathbf{p}};\hat{\mathbf{d}})+\mathbf{S}_B(x,\hat{\mathbf{p}};\hat{\mathbf{d}}), \quad (2.11)$$

where $S_A(x,\hat{\mathbf{p}},\hat{\mathbf{d}})$ [respectively, $S_B(x,\hat{\mathbf{p}},\hat{\mathbf{d}})$] is the part of the series (2.8) contributed by vectors $\mathbf{G}\in L^*$ with $\mathbf{G}\cdot\mathbf{d}=0$ (respectively $\mathbf{G}\cdot\mathbf{d}\neq 0$). CB of these two respective types is called type-*A* and type-*B* CB (with respect to $\hat{\mathbf{d}}$). From this definition and arguments similar to those adduced to arrive at Eq. (2.13), these types of coherent radiation from the above disordered IQC *K* have the following qualitative properties. Type-*A* CB is very intense at sufficiently small *positive* values of x when $\hat{\mathbf{p}}$ is almost, but not exactly, parallel to $\hat{\mathbf{d}}$ ($G_l\cong 0$), and is sensitively dependent on the angle between $\hat{\mathbf{p}}$ and $\hat{\mathbf{d}}$. On the other hand, for $\hat{\mathbf{p}}\cong\hat{\mathbf{d}}$, or even for $\hat{\mathbf{p}}=\hat{\mathbf{d}}$, type-*B* CB is significant only at much larger values of $x\ll 1$. It is generally much less intense than that of type-*A* and varies slowly with θ. These properties are similar to those of the corresponding types of CB in crystals [22].

We now mention an important property of type-*A* CB in *K* which could serve as its experimental signature. Consider a right-handed orthonormal basis $\{\hat{\mathbf{d}}_i\}_{i=1}^3$ for $\mathcal{E}$ such that $\hat{\mathbf{d}}_3=\hat{\mathbf{d}}$ is viewed as the polar axis. Let $0\leqslant\theta\leqslant\pi$ denote the angle between $\hat{\mathbf{p}}$ and $\hat{\mathbf{d}}_3$, and $0\leqslant\phi<2\pi$ that between the projection of $\hat{\mathbf{p}}$ into the $\hat{\mathbf{d}}_1,\hat{\mathbf{d}}_2$-plane and $\hat{\mathbf{d}}_1$. We have

$$\hat{\mathbf{p}}\cdot\mathbf{G}=\sin\theta(\cos\phi G_1+\sin\phi G_2)+\cos\theta G_3, \quad (2.12)$$

where $G_i=\mathbf{G}\cdot\hat{\mathbf{d}}_i$ $(i=1,2,3)$. Using the definition of $S_A(x,\hat{\mathbf{p}};\hat{\mathbf{d}})$, and taking into account Eqs. (2.9) and (2.7), the definitions $G_l=(\hat{\mathbf{p}}\cdot\mathbf{G})$, $G_t=(G^2-G_l^2)^{1/2}$, and Eq. (2.12), one concludes that if $\theta>0$ and $x>0$ are sufficiently small, then the approximate scaling law

$$S_A(x,\hat{\mathbf{p}};\hat{d})\cong(1/\sin\theta)f(x/\sin\theta,\phi) \quad (2.13)$$

holds for type-*A* CB emitted by relativistic electrons traversing *K*. A similar scaling law holds in the Born approximation for CB of this type occurring in a large class of QCs whose tiles are decorated more realistically than those of *K*. An analogous law that is predicted to hold for crystals has been verified experimentally for type-*A* CB emitted by electrons of about 3-MeV kinetic energy incident on Si crystals [28]. In these beautiful experiments, this law served to identify type-*A* CB.

III. NUMERICAL RESULTS ON TYPE-*A* CB FOR THE DISORDERED IQC MODEL *K*

In this section we will discuss results of numerical calculations of $S_A(x,\hat{\mathbf{p}};\hat{\mathbf{d}})$ and $S_B(x,\hat{\mathbf{p}};\hat{\mathbf{d}})$ for electrons of 5-MeV kinetic energy incident on *i*-Al-Mn-Si, described by the specialization of the *K* model (vertex model) in which a Mn atom is placed at each vertex of the disordered tiles of *K*. In these calculations, we assumed that $a=2^{1/2}\times 4.6$ Å (see Ref. [19]) and chose directions of incidence close to $\hat{\mathbf{i}}_3$, i.e., almost parallel to an axis of fivefold symmetry. Here $\{\mathbf{i}_j\}_{j=1}^3$ is the right-handed orthonormal basis of the physical space $\mathcal{E}$ mentioned in Appendix A. Hence we naturally chose $\hat{\mathbf{d}}_i=\hat{\mathbf{i}}_i$ $(i=1,2)$, $\hat{\mathbf{d}}_3=\hat{\mathbf{d}}=\hat{\mathbf{i}}_3$. Thus, the vectors $\mathbf{G}\in L^*$ [recall Eq. (2.2′)] involved in our calculations of $S_A(x,\hat{\mathbf{p}};\hat{\mathbf{d}})$ [respectively, $S_B(x,\hat{\mathbf{p}};\hat{\mathbf{d}})$] were those with $G_3=\mathbf{G}\cdot\hat{\mathbf{i}}_3=0$ (respectively, $G_3\neq 0$). A simple argument using Eq. (A1) in Appendix A, (2.2′), and the irrationality of $5^{1/2}$ show that $\mathbf{G}\in L^*$ is such that $G_3=0$ if and only if

$$\mathbf{G}=(2\pi/a)\sum_{i=1}^{4} m_i(\mathbf{e}_i-\mathbf{e}_5), \quad (3.1)$$

where $m_1,\ldots,m_4$ are arbitrary integers.

Since $\hat{\mathbf{d}}=\hat{\mathbf{i}}_3$ in this section, $S_A(x,\hat{\mathbf{p}};\hat{\mathbf{i}}_3)$ [respectively, $S_B(x,\hat{\mathbf{p}};\hat{\mathbf{i}}_3)$] will be abbreviated by $S_A(x,\hat{\mathbf{p}})$ [respectively, $S_B(x,\hat{\mathbf{p}})$] henceforth without fear of confusion. We will first review our numerical results for type-*A* CB and will then comment briefly on those for type-*B* CB. By the above discussion and the fact that $\tilde{\chi}(-\mathbf{G}')=\tilde{\chi}(\mathbf{G}')$ for $\mathbf{G}\in L^*$,

$$S_A(x,\hat{\mathbf{p}})=\sum_{\mathbf{G}\in L_0^*}\exp(-2B|\mathbf{G}|^2-2B'|\mathbf{G}'|^2)\times F(\mathbf{G},x,\hat{\mathbf{p}})|\tilde{\chi}(\mathbf{G}')|^2, \quad (3.2)$$

where L_0^* is the subset of L^* composed of vectors $\mathbf{G}$ of the form Eq. (3.1). Hence the sum in Eq. (3.2) can be written as a quadruply infinite sum over all integers $m_1,\ldots,m_4$. It was evaluated by using the truncation $|m_i|\leqslant 8$ $(i=1,\ldots,4)$ in most cases, but occasionally a higher-order truncation was employed. In Figs. 1 and 2, we depict results for $S_A(x,\hat{\mathbf{p}})$ in the interval $0\leqslant x\leqslant 0.005$, assuming that the parameters B,B' determining the phonon and phason Debye-Waller factors have the respective values 0.01 and 0.4 Å^2, in agreement with the widely held view that B' is usually much larger than B [29]. Indeed, values of B' as large as 1.35 have been advocated in the experimental literature [30]. Our calculations were performed using exact values of $\tilde{\chi}(\mathbf{G}')$ obtained from Elser's formula (C1) in Appendix C rather than by making the equivalent-sphere approximation, commonly employed to compute the intensity of the Bragg diffraction peaks of QCs [31]. This approximation consists of replacing the complicated exact expression for the Fourier transform $\tilde{\chi}$ of the characteristic function χ of $C(a)$ by that of a sphere of the same volume centered at the origin. Errors of about 10% would have been incurred by making it. An overall accuracy

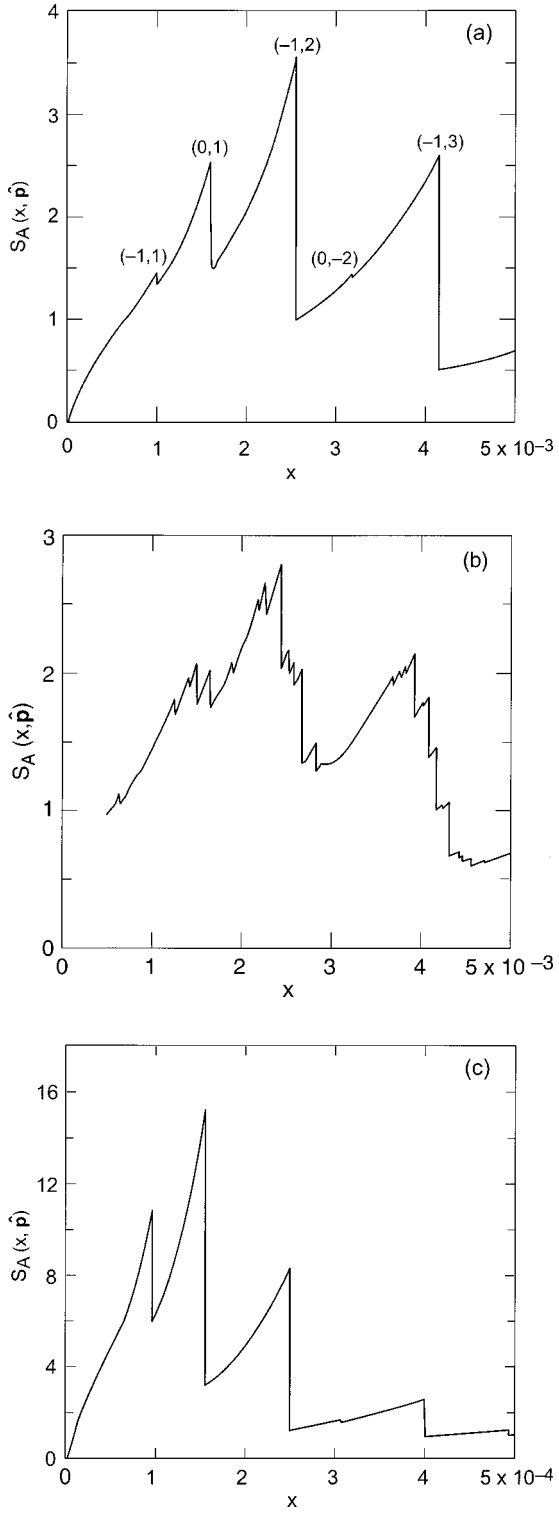

FIG. 1. $S_A(x,\hat{\mathbf{p}})$ vs x for electrons of 5-MeV kinetic energy incident on i-Al-Mn-Si (described by the model defined in the first paragraph of Sec. III) in a direction close to that of a fivefold axis. With θ,ϕ defined as in Sec. III (second sentence, third paragraph), parts (a)–(c) of the figure refer to the following cases: (a) $\theta=1°$, $\phi=0°$ $(0<x\leqslant 0.005)$; (b) $\theta=1°$, $\phi=2°$ $(0.0005\leqslant x\leqslant 0.005)$; (c) $\theta=1°$, $\phi=2°$ at very low photon energies $(0<x\leqslant 0.0005)$. Note that the missing part of the graph in Fig. 1(b) for $0<x\leqslant 0.0005$ is depicted in detail in Fig. 1(c).

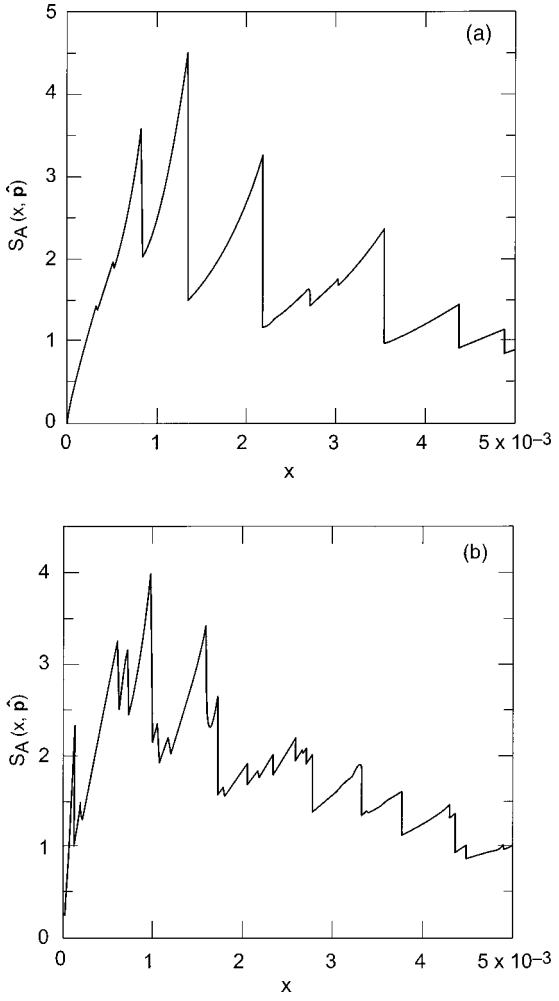

FIG. 2. $S_A(x,\hat{\mathbf{p}})$ vs x for electrons of 5-MeV kinetic energy incident on i-Al-Mn-Si (described by the model defined in the first paragraph of Sec. III) in a direction close to that of a fivefold axis. With θ,ϕ defined as in Sec. III (second sentence, third paragraph), parts (a) and (b) of the figure refer to the following cases: (a) $\theta=1°$, $\phi=18°$ $(0<x\leqslant 0.005)$; (b) $\theta=1°$, $\phi=13°$ $(0<x\leqslant 0.005)$.

better than 2% was achieved in the present calculations of $S_A(x,\hat{\mathbf{p}})$ by using Elser's formula and the above truncation.

A rich variety of type-A CB phenomena was revealed by these calculations. Before summarizing the results, we recall that in the present case $(\hat{\mathbf{d}}=\hat{\mathbf{i}}_3)$ θ,ϕ are the angles between $\hat{\mathbf{p}}$ and $\hat{\mathbf{i}}_3$, and between $\hat{\mathbf{i}}_1$ and the projection of $\hat{\mathbf{p}}$ into the $\hat{\mathbf{i}}_1,\hat{\mathbf{i}}_2$ plane, respectively. Figure 1(a) concerns the case when $\hat{\mathbf{p}}$ is given by $\theta=1°$, $\phi=0°$. It depicts three type-A macropeaks and two smaller peaks. In this case, each $k_{\mathbf{G}}(\hat{\mathbf{p}})$ $(\mathbf{G}\in L_0)$ depends on the m_i only through a unique pair of integers $\mu_1=m_1+m_4$, $\mu_2=m_2+m_3$ [property (1), Appendix D]. Hence, infinitely many different quadruplets m_1,m_2,m_3,m_4 correspond to each such $k_{\mathbf{G}}(\hat{\mathbf{p}})$, which accounts for the large vertical drops depicted in Fig. 1(a) [23]. The pairs μ_1,μ_2 labeling the peaks in this figure are as indicated there. More generally [properties (2) and (3), Appendix D], for arbitrary $\theta>0$ a necessary condition for each such quadruplet to possess this property is that

$$s \tan \phi = \alpha + \sqrt{5}\beta, \tag{3.3}$$

where $s = \sin(2\pi/5)$ and α,β are rationals. In more detail [property (3), Appendix D], when Eq. (3.3) does not hold, *exactly one* quadruplet $m_1,\ldots,m_4$ corresponds to each $k_{\mathbf{G}}(\hat{\mathbf{p}})$ ($\mathbf{G} \in L_0{}^*$). When $\hat{\mathbf{p}}$ is changed to $\theta = 1°$, $\phi = 2°$, one sees from Fig. 1(b) that the drops in the three largest peaks in Fig. 1(a) become ''fragmented'' into smaller drops, and Fig. 1(c) shows that several very large peaks appear at extremely small x values ($0 < x \leqslant 0.0005$) when this change is made. The smallness of these drops is expected since $\phi = 2°$ violates (3.3) [32], which implies that the drops are due to the loss of only one term of the sum (3.2). As to the low-energy type-*A* peaks in Fig. 1(c), our theory predicts their occurrence for $\theta > 0$ when $\phi > 0$ is small enough. The vectors $\mathbf{G} \in L_0{}^*$ contributing to them are overwhelmingly those for which $m_3 = -m_2$, $m_4 = -m_1$, where m_1, m_2 are suitable positive integers.

It is well known that the Landau-Pomeranchuk-Migdal (LPM) and dielectric supression effects [12,13] can act to reduce very soft bremsstrahlung emission. As discussed in Appendix E, we expect that the LPM effect will not reduce any of the peaks in Figs. 1 or 2, and that dielectric suppression will affect at most the lowest peak in Fig. 1(c).

Figures 2(a) and 2(b) depict results for the respective cases $\theta = 1°$, $\phi = 18°$ and $\theta = 1°$, $\phi = 13°$. In the first case, ϕ satisfies Eq. (3.3) [33] and macropeaks with ''clean'' vertical drops are very much in evidence, as in Fig. 1(a). In the second case, ϕ does not satisfy it, and the drops are fragmented, similarly to those shown in Fig. 1(b). Fragmentation was also detected in another case in which Eq. (3.3) is violated, namely, $\theta = 1°$, $\phi = 15°$.

The results in Figs. 1 and 2 are fairly insensitive to rather large variations in B and B'. For example, decreasing B' from 0.4 to 0.1 Å^2 while keeping $B = 0.01$ Å^2 increased the intensity of the highest peak in Fig. 1 by only 17%. On the other hand, setting $B = 0.001$ while keeping $B' = 0.4$ Å^2 increased this intensity by only 16%. The qualitative shape of the graph of $S_A(x,\hat{\mathbf{p}})$ in Fig. 1(a) and the positions of the vertical drops in this figure were *unchanged* by these variations.

Finally, a spot check of the accuracy of the experimentally significant scaling law (2.13) for type-*A* CB at $x = 0.005$ and $\phi = 0$ showed that in this case the value of $S_A(x,\hat{\mathbf{p}})$ is 0.8599 (respectively, 0.4299) for $\theta = 1°$ (respectively, $\theta = 2°$), in excellent agreement with this law.

We now turn to the results for $S_B(x,\hat{\mathbf{p}})$ obtained by summing the sixfold infinite series representing it. We confine our remarks to the case $\theta = 1°$, $\phi = 0$. Since the calculation of a reasonably detailed graph for $S_B(x,\hat{\mathbf{p}})$ would have taken an unreasonably long time with the computer facilities at our disposal, we only performed spot evaluations of this quantity. For $0 \leqslant x \leqslant 0.005$, the ratio of $S_B(x,\hat{\mathbf{p}})$ to the maximum value of $S_A(x,\hat{\mathbf{p}})$ in this interval was found to be less than 4%. Spot checks in the interval $0.005 \leqslant x \leqslant 0.100$ indicate that $S_A(x,\hat{\mathbf{p}}) + S_B(x,\hat{\mathbf{p}})$ lies between 0.2 and 0.5 there, and thus that in the latter interval both $S_A(x,\hat{\mathbf{p}})$ and $S_B(x,\hat{\mathbf{p}})$ are small in comparison with the said maximum value.

IV. CONCLUDING REMARKS

We have developed a Born-approximation theory of CB emission by relativistic electrons traversing the primitive model of *i*-Al-Mn-Si (vertex model), in which a Mn atom is placed at each vertex of the Ammann rhombohedrons. The structure of *i*-Al-Mn-Si has been investigated by x-ray and neutron-diffraction experiments, whose results have been interpreted in the framework of the theory of atomic hypersurfaces. This has led to the following conclusions: the rhombohedral vertices are occupied with very high probability by Mn atoms, positions on the faces are occupied with a certain frequency of occurrence by Al atoms, and Si atoms are placed at three different sites along the long diagonal of the prolate rhombohedrons [19]. How well should one expect that the cross section $d\tilde{\sigma}_{\mathrm{CB}}/dk$, differential with respect to the photon energy k, for CB production in real *i*-Al-Mn-Si QCs be approximated by Eq. (2.8)? Briefly, for $\hat{\mathbf{p}}$ close to a major axis, one expects that the largest CB peaks in $d\tilde{\sigma}_{\mathrm{CB}}/dk$ occur at the same values of x and have the same shapes, qualitatively speaking, as those predicted by Eq. (2.8), but that they differ from them quantitatively. The reason for this is twofold. First, the summands on the right-hand-side (rhs) of the Born series (2.8) and those in the corresponding series for $d\tilde{\sigma}_{\mathrm{CB}}/dk$ run over all $\mathbf{G} \in L^*$ and are given by a product of a function of $\mathbf{G},\mathbf{x},\hat{\mathbf{p}}$ independent of the atomic decoration times the intensity of the Bragg diffraction spot at $\mathbf{G} \in L^*$. [This follows by arguments of the type used to prove Eq. (2.8) in Appendix B] Second, one expects that if there is a prominent Bragg peak of the vertex model indexed by a given $\mathbf{G} \in L^*$, then a large Bragg peak will appear for the same $\mathbf{G}$ in the case of its more realistic counterpart, but that the intensities of corresponding Bragg reflections for the two models will generally be different, due to the difference in decorations [34].

Needless to say, detailed formulas for CB production by relativistic electrons incident on realistically decorated models of *i*-Al-Mn-Si and other IQCs could be obtained, straightforwardly but tediously, by the methods of the present paper. Rather than dwelling on this matter, we close this section by mentioning an important topic not considered in this paper. Since x-ray diffraction experiments show that IQCs with little or no phason disorder exist in nature [35], it would be very interesting to measure the CB cross section, a differential with respect to k, for such materials and compare it with the corresponding theoretical results. The problem is that the Born series for this cross section converges very slowly or not at all for such IQCs, due to the smallness of their B'-values. The theoretical challenge is to devise a rigorously justified method for accelerating its numerical convergence.

ACKNOWLEDGMENTS

R.F. wishes to acknowledge funding by the Office of Naval Research through the Office of Naval Technology. A. W.S. wishes to thank Professor H.-D. Carstanjen, Professor A. Richter, and Professor H.-R. Trebin, as well as Dr. T. Kupke and Dr. W. Sigle, for useful conversations, and Professor A. Seeger for financial support during two visits to the

Max Planck Institute in Stuttgart. Last but not least, the authors are indebted to Professor H. L. Crannell, Dr. V. L. Jacobs, Dr. I. Mazin, Dr. T. Picraux, and Professor H. Überall for valuble remarks.

APPENDIX A: AUXILIARY QUASICRYSTALLOGRAPHIC FORMULAS

Set $\mathbf{e}_i=\Pi\boldsymbol{\varepsilon}_i$, $\mathbf{e}'_i=\Pi'\boldsymbol{\varepsilon}_i$ $(i=1,\ldots,6)$, where $\{\boldsymbol{\varepsilon}_i\}_{i=1}^6$ is the standard basis of $\mathbb{R}^6$ and Π' the projection complementary to Π. Using a convenient orthonormal basis $\{\mathbf{i}_j\}_{j=1}^3$ in $\mathcal{E}$, such that $\mathbf{i}_3$ is parallel to $\mathbf{e}_6$, which in turn is parallel to a fivefold symmetry axis, we can write

$$\mathbf{e}_i=(10)^{-1/2}(2\cos(2\pi i/5),2\sin(2\pi i/5),1)\quad(i=1,\ldots,5),$$

$$\mathbf{e}_6=(0,0,2^{-1/2}), \tag{A1}$$

where $(x_1,x_2,x_3)=\Sigma_{j=1}^3 x_j\mathbf{i}_j$. In terms of a suitable orthonormal basis $\{\mathbf{i}'_j\}_{j=1}^3$ of $\mathcal{E}'$, and writing $(x'_1,x'_2,x'_3)=\Sigma_{j=1}^3 x'_j\mathbf{i}'_j$, the vectors e'_i can be expressed in the form (A1), but with $\mathbf{e}_1,\mathbf{e}_2,\mathbf{e}_3,\mathbf{e}_4,\mathbf{e}_5,\mathbf{e}_6$ replaced by $\mathbf{e}'_1,\mathbf{e}'_4,\mathbf{e}'_2,\mathbf{e}'_5,\mathbf{e}'_3,-\mathbf{e}'_6$, respectively.

APPENDIX B: DERIVATION OF THE CROSS-SECTION FORMULA (2.8)

As a first step for deriving this formula for the K model, we make some remarks on the K_0 model. Directly from the definition of $\mathcal{K}$ and K_0 in Sec. II A, it follows that the atomic density of K_0 is given by

$$\rho(\mathbf{x})=\sum_{\mathbf{X}\in L}\delta(\mathbf{x}-\mathbf{X})\chi(-\mathbf{X}'). \tag{B1}$$

where L is defined by Eq. (2.2a), χ is the characteristic function of $C(a)$, and $\mathbf{X},\mathbf{X}'$ are complementary vectors. The interaction potential of an electron with the atoms in K_0 is assumed to have the form

$$V(\mathbf{x})=\sum_{\mathbf{X}\in L}v(\mathbf{x}-\mathbf{X})\chi(-\mathbf{X}'), \tag{B2}$$

where $v(\mathbf{x})$ is the value of the shielded Coulomb potential of an atomic nucleus at the origin acting on an electron at $\mathbf{x}\in\mathcal{E}$, which we assume to be of the Thomas-Fermi-Molière form. Note that

$$V(\mathbf{x})=\int_{\mathcal{E}}v(\mathbf{x}-\mathbf{y})\rho(\mathbf{y})d\mathbf{y}. \tag{B3}$$

By standard results of quantum electrodynamics [36], the differential cross section for the process $\mathbf{p}\to\mathbf{p}'+\mathbf{k}$ in which an unpolarized electron of momentum $\mathbf{p}$ traveling through K_0 produces a bremsstrahlung photon and a scattered electron of momenta $\mathbf{k}$ and $\mathbf{p}'$, respectively, is given by [21]

$$d^6\sigma/d\mathbf{k}d\mathbf{p}'=|\tilde{V}(\mathbf{q})|^2\mathscr{M}a(\mathbf{p},\mathbf{p}',\mathbf{k})\,\delta(E-E'-k) \tag{B4}$$

to order $\alpha^2(\alpha\cong 1/137)$. Here $\mathbf{q}=\mathbf{p}-\mathbf{p}'-\mathbf{k}$, and we recall that $k=|\mathbf{k}|$, $\mathbf{k}$ are the respective photon energy and momentum and that $E=(p^2+m^2)^{1/2}$, $E'=(p'^2+m^2)^{1/2}$ are the initial and final electron energies, respectively, with $p=|\mathbf{p}|$, $p'=|\mathbf{p}'|$, and with m the electron rest mass:

$$\tilde{V}(\mathbf{q}')=\int_{\mathcal{E}}\exp(-i\mathbf{q}'\cdot\mathbf{x})V(\mathbf{x})d\mathbf{x} \tag{B5}$$

(see Ref. [27]); and the function $\mathscr{M}$ is independent of K_0 and V, and contains no delta functions. By the definition of $K_\mathbf{w}$ in Sec. II A, it follows that the atomic density $\rho_\mathbf{w}(\mathbf{x})$ and interaction potential of an electron with the atoms of $K_\mathbf{w}$ are defined by the respective formulas

$$\rho_\mathbf{w}(\mathbf{x})=\sum_{\mathbf{X}\in L}\delta(\mathbf{x}-\mathbf{X}=\mathbf{u}(\mathbf{X}))\chi(-\mathbf{X}'-\mathbf{u}'(\mathbf{X}')), \tag{B6}$$

$$V_\mathbf{w}(\mathbf{x})=\sum_{\mathbf{X}\in L}v(\mathbf{x}-\mathbf{X}-\mathbf{u}(\mathbf{X}))\chi(-\mathbf{X}'-\mathbf{u}'(\mathbf{X}'))$$

$$=\int_{\mathcal{E}}v(\mathbf{x}-\mathbf{y})\rho_\mathbf{w}(\mathbf{y})d\mathbf{y}. \tag{B7}$$

By the second equality (B7), the Fourier transform of $V_\mathbf{w}$ can be expressed as

$$\tilde{V}_\mathbf{w}(\mathbf{q}')=(2\pi)^{-3/2}\tilde{v}(\mathbf{q}')\tilde{\rho}_\mathbf{w}(\mathbf{q}'). \tag{B8}$$

By definition, the cross section for the above bremsstrahlung process $\mathbf{p}\to\mathbf{p}'+\mathbf{k}$ in K is given by Eq. (B4), but with $|\tilde{V}(q)|^2=(2\pi)^{-3}|\tilde{v}(\mathbf{q})|^2|\tilde{\rho}(\mathbf{q})|^2$ replaced by $\langle|\tilde{V}_\mathbf{w}(q)|^2\rangle=(2\pi)^{-3}\cdot|\tilde{v}(\mathbf{q})|^2\langle|\tilde{\rho}_\mathbf{w}(\mathbf{q})|^2\rangle$, where $\langle\,\rangle$ is an appropriate Gaussian average [20] over the random variables $\mathbf{w}$. More specifically,

$$\langle|\tilde{\rho}_\mathbf{w}(\mathbf{q})|^2\rangle=N\frac{(2\pi)^3}{a^6V(a)}\sum_{\mathbf{G}\in L^*}\delta(\mathbf{q}-\mathbf{G})|\tilde{\chi}(-\mathbf{G}')|^2$$
$$\times\exp(-2B|\mathbf{G}|^2-2B'|\mathbf{G}'|^2)+\cdots, \tag{B9}$$

where the sum ranges over the set L^* defined by Eq. (2.2′), N is the number of atoms in K, $V(a)$ the volume of $C(a)$, and $\exp(-2B|\mathbf{G}|^2)$ and $\exp(-2B'|\mathbf{G}'|^2)$ the respective Deybe-Waller factors arising from phonon and phason fluctuations. The terms on the rhs of Eq. (B9) involving delta functions $\delta(\mathbf{q}-\mathbf{G})=\delta(\mathbf{p}-\mathbf{p}'-\mathbf{k}-\mathbf{G})$ are the only ones contributing to coherent bremsstrahlung, since those denoted by ''$+\cdots$'' contain no delta functions involving $\mathbf{q}$, and thus can only contribute to incoherent bremsstrahlung.

In summary, the cross section for an unpolarized electron in K with momentum $\mathbf{p}$ to produce a *coherent* bremsstrahlung photon and an electron with momenta $\mathbf{k},\mathbf{p}'$, respectively, can be written as

$$d^6\sigma_{\mathrm{CB}}/d\mathbf{k}d\mathbf{p}'=(2\pi)^{-3}|\tilde{v}(\mathbf{q})|^2\langle|\tilde{\rho}_\mathbf{w}(\mathbf{q})|^2\rangle_0\mathscr{M}(\mathbf{p},\mathbf{p}',\mathbf{k})$$
$$\times\delta(E-E'-k) \tag{B10}$$

to order α^2, where $\langle|\tilde{\rho}_\mathbf{w}(\mathbf{q})|^2\rangle_0$ denotes the terms in the rhs of Eq. (B9) preceding ''$+\cdots$''.

In the small-angle and high-energy approximations [37], which are accurate enough for our purposes, we arrive at the desired formula (2.8) by using Eqs. (B10) and (2.3), the definition of $\langle|\tilde{\rho}_{\mathbf{w}}(q)|^2\rangle_0$, and the expression for $\mathscr{M}$ [36], after tedious but straightforward calculations.

APPENDIX C: EXACT FORMULA FOR $\tilde{\chi}(\mathbf{G}')$

The Fourier transform [27] of the characteristic function χ of the triacontahedron $C(a)$ is a real-valued function given by [38]

$$\tilde{\chi}(\mathbf{G}')/a^3=\sum_{1\leqslant i<j<k\leqslant 6} S_1(i,j,k)S_2(i,j,k), \tag{C1}$$

where $\mathbf{G}'=(2\pi/a)\Sigma_{i=1}^{6}m_i\mathbf{e}_i'$, as before. We note that the rhs of (C1) is independent of a. For $1\leqslant i<j<k\leqslant 6$,

$$S_1(i,j,k)=v_{\mathrm{lmn}}(\sin z_l/z_l)(\sin z_m/z_m)(\sin z_n/z_n),$$

$$S_2(i,j,k)=\left(\frac{4}{5}-\frac{2}{5}\sigma_{ijk}\right)\cos z_i\cos z_j\cos z_k,$$
$$+\left(\frac{1}{5}+\frac{2}{5}\sigma_{ijk}\right)\cos(\sigma_{jk}z_i+\sigma_{ki}z_j+\sigma_{ij}z_k, \tag{C2}$$

where i,j,k,l,m,n is a permutation of 1, 2, 3, 4, 5, 6 and $\sin z/z$ is defined as unity when $z=0$.

The significance of the other symbols in Eq. (C2) is as follows. For $1\leqslant i<j<k\leqslant 6$, v_{ijk} denotes the volume of the rhombohedron with edges $\mathbf{e}'_i,\mathbf{e}'_j,\mathbf{e}'_k$:

$$v_{ijk}=\frac{(5^{1/2}-\sigma_{ijk})}{2\times 5^{3/4}}, \tag{C3}$$

where we recall that $\mathbf{e}'_i=\Pi'\boldsymbol{\varepsilon}_i$ and where $\sigma_{ijk}=\sigma_{ij}\sigma_{jk}\sigma_{ki}$, with $\sigma_{ij}=\sigma_{ji}=\mathrm{sign}(\mathbf{e}'_i,\mathbf{e}'_j)$ $(i,j=1,\ldots,6)$. Explicitly,

$$[\sigma_{ij}]_{i,j=1,\ldots,6}=\begin{bmatrix} 1 & -1 & 1 & 1 & -1 & -1\\ -1 & 1 & -1 & 1 & 1 & -1\\ 1 & -1 & 1 & -1 & 1 & -1\\ 1 & 1 & -1 & 1 & -1 & -1\\ 1 & 1 & -1 & 1 & -1 & -1\\ -1 & 1 & 1 & -1 & 1 & -1\\ -1 & -1 & -1 & -1 & -1 & 1 \end{bmatrix}, \tag{C4}$$

as follows directly, but tediously, from the formulas for the $\mathbf{e}_i'$ obtainable from Appendix A. Finally, for $i=1,\ldots,6$,

$$z_i=\frac{\pi}{2}\left[m_i+5^{-1/2}\sum_{j=i,\ j=1,\ldots,6}\sigma_{ij}m_j\right]. \tag{C5}$$

APPENDIX D: PROOF OF CERTAIN PROPERTIES OF $k_{\mathbf{G}}(\hat{\mathbf{p}})$ $(\mathbf{G}\in L_0^*)$ FOR $\hat{\mathbf{d}}=\hat{\mathbf{i}}_3$

This appendix is devoted to proving properties of these cutoffs which are needed in Sec. III. Of course, in this appendix we choose $\hat{\mathbf{d}}_i=\hat{\mathbf{i}}_i$ $(i=1,2)$, $\hat{\mathbf{d}}=\hat{\mathbf{d}}_3=\hat{\mathbf{i}}_3$, where the orthonormal bases $\{\hat{\mathbf{d}}_i\}_{i=1}^3$ and $\{\hat{\mathbf{i}}_i\}_{i=1}^3$ are defined in Sec. III and Appendix A, respectively. Thus, $\hat{\mathbf{d}}$ is parallel to a fivefold axis. Denoting by θ,ϕ the polar and azimuthal angles of $\hat{\mathbf{p}}$ defined in Sec. III [second sentence of the paragraph containing Eq. (3.3)], we proceed to prove the following three properties of $k_{\mathbf{G}}(\hat{\mathbf{p}})$ $(\mathbf{G}\in L_0^*)$. [Recall the definition of L_0^* after Eq. (3.2).]

(1) If $\theta>0$ and $\phi=0$, then each such $k_{\mathbf{G}}(\hat{\mathbf{p}})$ depends on the m_i [recall Eq. (3.1)] only through $\mu_i=m_i+m_4$ and $\mu_2=m_2+m_3$.

To prove this and other properties asserted in this appendix, we will need the fact that the components $G_i=\mathbf{G}\cdot\hat{\mathbf{d}}_i$ $(i=1,2,3)$ of $\mathbf{G}\in L_0^*$ are given by

$$G_1=(2\pi/a)\sqrt{2/5}[(c-1)(m_1+m_4)+(c'-1)(m_2+m_3)], \tag{D1a}$$

$$G_2=(2\pi/a)\sqrt{2/5}s[(m_1-m_4)+2c(m_2-m_3)], \tag{D1b}$$

$$G_3=0. \tag{D1c}$$

where $c=\cos(2\pi/5)$, $c'=\cos(4\pi/5)$, $s=\sin(2\pi/5)$. This follows, in particular, from Eqs. (3.1) and (A1), and the definition of L_0^*. By Eqs. (2.12) and (D1c),

$$\mathbf{P}\cdot\mathbf{G}=\sin\theta(G_1\cos\phi+G_2\sin\phi). \tag{D2}$$

Property (1) follows immediately from Eqs. (D1), (D2), and (2.5).

(2) If $s\tan\phi=\alpha+\sqrt{5}\beta$, where $\alpha,\beta\in\mathbf{Q}$, the rationals, then to each value of $k_{\mathbf{G}}(\hat{\mathbf{p}})$ $(\mathbf{G}\in L_0^*)$ there corresponds a denumerably infinite number of distinct vectors $(m_1,m_2,m_3,m_4)\in\mathbf{Z}^4$.

We will prove this property by showing that under the stated hypothesis the equation $\hat{\mathbf{p}}\cdot\mathbf{G}=0$ is satisfied by a denumerably infinite number of distinct vectors $\mathbf{G}\in L_0^*$. Henceforth, we assume that $\mathbf{G}$ obeys this last relation.

By Eqs. (D1a), (D1b), (D2), and $s\tan\phi=\alpha+\sqrt{5}\beta$, it follows that $\mathbf{p}\cdot\mathbf{G}=\gamma+\sqrt{5}\delta$, where $\gamma,\delta\in\mathbf{Q}$, and thus $\mathbf{p}\cdot\mathbf{G}=0$ is equivalent to the pair of equations $\gamma=0$, $\delta=0$. If in addition $\sin\theta\cos\phi\neq 0$, these equations are equivalent to the matrix equation

$$Mm=0, \tag{D3}$$

where $m=\mathrm{col}(m_1,m_2,m_3,m_4)$ and M is a 2×4 matrix over $\mathbf{Z}$ of rank 2 depending on α,β. It follows [39] that there exist a 2×2 matrix $A\in GL(2,\mathbf{Z})$ and a 4×4 matrix $B\in GL(4,\mathbf{Z})$ such that

$$AMB=\begin{bmatrix}\delta_1 & 0 & 0 & 0\\ 0 & \delta_2 & 0 & 0\end{bmatrix}.$$

Here δ_1,δ_2 are unique positive integers (invariant factors of M) such that δ_1 divides δ_2. Therefore, the most general $(m_1,m_2,m_3,m_4)\in\mathbf{Z}^4$ satisfying Eq. (D3) is given by

$$m_i = \sum_{j=3,4} B_{ij} n_j \quad (i=1,\ldots,4), \tag{D4}$$

where n_3, n_4 are arbitrary integers. This completes the proof of property (2).

(3) Let $s \tan\phi \notin \mathbf{Q}(\sqrt{5})$, where $\mathbf{Q}(\sqrt{5}) = \{\rho + \sqrt{5}\sigma : \rho, \sigma \in \mathbf{Q}\}$. Then to each value of $k_{\mathbf{G}}(\hat{\mathbf{p}})$ ($\mathbf{G} \in L_0{}^*$) there corresponds exactly one $(m_1, m_2, m_3, m_4) \in \mathbf{Z}^4$.

The proof is similar, but much simpler than that of property (2).

APPENDIX E: LPM AND DIELECTRIC SUPPRESSION EFFECTS ON LOW-ENERGY CB EMISSION FROM *i*-AL-MN-SI [40]

The Landau-Pomeranchuk-Migdal (LPM) effect [12,13] is the suppression of low-energy bremsstrahlung photons because of multiple scattering of the incident electron within a distance known as the (radiation) formation length $l_f = 2\gamma^2/k$ (see Ref. [21]). Originally, the phenomenon was only considered for ordinary bremsstrahlung, but the basic arguments involved also apply to CB in QCs, to which we confine ourselves henceforth. In order for the latter radiation to be significantly LPM suppressed, the condition $x = k/E < E/E_{\mathrm{LPM}}$ should be satisfied. For a monoatomic material, $E_{\mathrm{LPM}}(\mathrm{eV}) = 3.8\times 10^{12} X_0(\mathrm{cm})$, where X_0 is the radiation length $137/2zr_0^2 n \log(183 z^{-1/3})$, with n the number of atoms per cm^3, z their atomic number, and r_0 the classical electron radius. For i-$Al_{74}Mn_{20}Si_6$, an upper bound for E_{LPM} is 1.6×10^7 MeV (the value of E_{LPM} for solid Mn). Hence a necessary condition for CB from 5-MeV kinetic energy electrons to experience large LPM suppression in this QC is that $x < 3.4\times 10^{-7}$. We thus conclude that this does not occur for any of the CB peaks in Figs. 1 and 2.

Dielectric suppression [12,13] takes place because of the interaction of the bremsstrahlung photons with the electrons in the medium via Compton scattering. This interaction can be coherent for forward scattering, producing a photon phase shift. If this phase shift is large enough over the formation length, then a loss in coherence results which reduces photon emission. A necessary condition for large dielectric suppression is that $x < \omega_p/m$, where $\omega_p = \sqrt{4\pi N \langle z\rangle e^2/m}$ is the plasma frequency and $\langle z\rangle$ the average value of the atomic number z in the medium. For i-$Al_{74}Mn_{20}Si_6$, this condition becomes $x < 0.82\times 10^{-4}$, i.e., $k < 0.45$ keV for the case of 5-MeV kinetic energy electrons of interest here. Thus, none of the CB peaks depicted in the figures are significantly reduced by dielectric suppression, except possibly the lowest-energy peak in Fig. 1(c).

With modern detection devices, one can measure x rays of energies as low as 0.5 keV [40]. We also remark that very few of the peaks in Figs. 1 and 2 lie close to the absorption edges of Al, Si, and Mn [41]. This is fortunate, since the corresponding characteristic x rays could impede their direct observation. However, we note that the scaling law (2.13) could be used to find such CB peaks indirectly by varying θ, keeping ϕ and E fixed, in a way similar to that used by Watson and Koehler [42].

[1] For general surveys of CB and CR in crystals, see *Coherent Radiation Sources*, edited by A. W. Sáenz and H. Überall, Topics in Current Physics Vol. 38 (Springer-Verlag, Berlin, 1985); M. A. Kumakhov and G. Shirmer, *Atomic Collisions in Crystals* (Gordon and Breach, New York, 1980); M. A. Kumakhov and F. F. Komarov, *Radiation from Charged Particles in Solids* (American Institute of Physics, New York, 1991).

[2] J. U. Andersen, Nucl. Instrum. Methods **170**, 1 (1980).

[3] The type of CB due to free-bound transitions was first studied experimentally by the Aarhus group. See J. U. Andersen, E. Bonderup, E. Læggsgaard, B. B. Marsh, and A. H. Sørensen, Nucl. Instrum. Methods Phys. Res. **194**, 209 (1982). For the theory, see A. W. Sáenz, A. Nagl, and H. Überall, Phys. Rev. B **37**, 7239 (1988).

[4] For more careful definitions of type-*A* and type-*B* CB in crystals and for statements of their basic properties, see A. W. Sáenz and H. Überall, Phys. Rev. B **25**, 4418 (1982).

[5] T. Kupke and H.-R. Trebin, J. Phys. I **3**, 1629 (1993).

[6] W. Sigle and H. D. Carstanjen, Philos. Mag. B **66**, 533 (1992). In these experiments, the CB photon intensity was measured as a function of photon energy for **p** oriented along various quasicrystalline axes, keeping fixed the angle between **p** and the direction of the detected photons. This contrasts with the present work, which is concerned with the CB intensity integrated over angles.

[7] For general surveys of quasicrystals, see *The Physics of Quasicrystals*, edited by P. J. Steinhardt and S. Ostlund (World Scientific, Singapore, 1987); *Aperiodicity and Order*, edited by M. V. Jarić (Academic, Boston, 1989), Vols. 1 and 2,; *Aperiodicity and Order*, edited by M. V. Jarić and D. Gratias (Academic Press, Boston, 1989) Vol. 3; and C. Janot, *Quasicrystals, A Primer* (Clarendon Press, Oxford, 1992).

[8] Phasons are discussed, e.g., by J. E. S. Socolar, T. C. Lubensky, and P. J. Steinhardt, Phys. Rev. B **34**, 3345 (1986).

[9] For the purposes of this paper, the distinction between the various members of the *i*-Al-Ma-Si family, such as $Al_4Mn_{20}Si_6$, $A_{74}Mn_{21}Si_5$, etc. is not important.

[10] T. Kupke, U. Peschke, H.-D. Carstanjen, and H.-R. Trebin, Phys. Rev. B **43**, 13 758 (1991). See also W. Steurer, Mater. Sci. Forum **150–151**, 15 (1994).

[11] See, e.g., C. Janot and J. M. Dubois, J. Phys. F **18**, 2303 (1988), particularly pp. 2317, 3218, and 2324.

[12] M. L. Ter-Mikaelian, *High-Energy Electromagnetic Processes in Condensed Media* (Wiley, New York, 1972).

[13] P. L. Anthony *et al.*, Phys. Rev. D **56**, 1373 (1997).

[14] A. Katz and M. Duneau, J. Phys. (Paris) **47**, 181 (1986).

[15] V. Elser, Acta Crystallogr., Sect. A: Found. Crystallogr. **42**, 36 (1986).

[16] R. Kramer and R. Neri, Acta Crystallogr., Sect. A: Found. Crystallogr. **40**, 580 (1984).

[17] V. Elser, Phys. Rev. B **32**, 4892 (1985).

[18] D. Levine and P. J. Steinhardt, Phys. Rev. B **34**, 82 (1986).

[19] See T. Kupke *et al.* in Ref. [10].
[20] M. V. Jarić and D. R. Nelson, Phys. Rev. B **37**, 4458 (1988).
[21] We use units in which $\hbar = c = 1$.
[22] See, e.g., A. W. Sáenz and H. Überall in Ref. [4].
[23] The verticality of these drops depicted in, e.g., Fig. 1(a), results from using the approximate formula (2.5) to calculate the cutoffs $k_{\mathbf{G}}(\hat{\mathbf{p}})$, but small deviations from verticality occur in the multi-MeV electron energy regime when $k_{\mathbf{G}}(\hat{\mathbf{p}})$ is calculated exactly. These deviations are probably undetectable experimentally in the cases considered in this paper.
[24] An analog of Eq. (2.8) for crystals was derived by H. Überall, Phys. Rev. **103**, 1055 (1956). See, also, G. D. Palazzi, Rev. Mod. Phys. **40**, 611 (1968). The corresponding formula without making these approximations was obtained by A.W.S. in unpublished work (1971), and is stated in the paper by A. W. Sáenz and H. Überall in Ref. [4].
[25] These two types of Debye-Waller factors are commonly used to analyze the effect of phonon and phason fluctuations in diffraction data from quasicrystalline targets. For a state-of-the art example, see M. V. Jarić and S.-Y. Qui, Phys. Rev. A **24**, 861 (1981). In the literature, B' is frequently denoted by $B_{\perp}$.
[26] D. S. Gemell, Rev. Mod. Phys. **46**, 129 (1974).
[27] If f is a function from $\mathcal{E}$ onto $\mathbf{C}$, we denote its Fourier transform by $\tilde{f}(\mathbf{y}) = \int_{\mathbf{k}^3} \exp(-i\mathbf{y}\cdot\mathbf{x}) f(\mathbf{x}) d\mathbf{x}$, with no factors $(2\pi)^{-3/2}$, etc. in front of the integral. Similar definitions apply to functions $f: \mathcal{E}' \to \mathbf{C}$ and distributions.
[28] J. L. Watson and J. S. Koehler, Phys. Rev. A **24**, 861 (1981); Phys. Rev. B **25**, 3079 (1982).
[29] See, e.g., M. V. Jarić and S.-Y. Qui in Ref. [25].
[30] M. de Boissieu, P. Stephens, M. Boudard, C. Janot, D. L. Chapman, and M. Audier, Phys. Rev. Lett. **72**, 3538 (1994).
[31] See, e.g., J. W. Cahn and D. Gratias, J. Phys. (Paris), Colloq. **47**, C3-415 (1986), particularly p. 417.
[32] The fact that (3.3) is violated at the values of ϕ mentioned in the text follows by using Theorem 3.11, p. 39 of I. Niven, *Irrational Numbers*, Carus Mathematical Monograph No. 11 (Quinn and Boden Co., Inc., Rahway, NJ, 1967).
[33] Indeed, the left-hand side of Eq. (3.3) equals $(1/4)(-1+\sqrt{5})$ for $\phi = 18°$ by elementary properties of the regular pentagon.
[34] This expectation is strongly supported by the remarkable qualitative agreement of experimental diffraction patterns of the closely related QC *i*-Mn-Si with the corresponding calculated patterns for the vertex model, neglecting phonon, and phason disorder. See V. Elser, Ref. [17], particularly Figs. 9–11.
[35] M. Cornier-Quiquandon *et al.*, Phys. Rev. B **44**, 2071 (1991).
[36] See, e.g., A. J. Akhiezer and V. B. Berestetskii, *Quantum Electrodynamics* (Interscience, New York, 1965), Sec. 29.2.
[37] See the paper of H. Überall in Ref. [24].
[38] See Part 2 of the Appendix of Ref. [15], where it should be noted that some of the symbols have a different meaning from those in the present appendix.
[39] See, e.g., S. MacLane and G. Birkhoff, *Algebra* (Macmillan, New York, 1967), Theorem 18, p. 366. See also Theorem 15, p. 361.
[40] H. L. Crannell (private communication).
[41] See, e.g., *American Institute of Physics Handbook*, 3rd ed. (McGraw-Hill, New York, 1972), pp. **7**-98.
[42] See, e.g., J. L. Watson and J. S. Koehler, Phys. Rev. A **24**, 861 (1981), especially Fig. 2.